Journal of the Korean Physical Society
https://doi.org/10.1007/s40042-025-01493-5

Online ISSN 1976-8524
Print ISSN 0374-4884

RESEARCH - COSMOLOGY, ASTROPHYSICS, AND PLANETARY SCIENCE

Buchdahl gravastars

Mahesh Kumar[1] · S. Surendra Singh[1] · Meghanil Sinha[1] · Javlon Rayimbaev[2,3] · Inomjon Ibragimov[4]

Received: 15 July 2025 / Revised: 10 September 2025 / Accepted: 18 September 2025

Abstract

We present a new stellar model which employs the Buchdahl metric potential for the temporal metric potential in the spherical symmetric configuration, following the Mazur–Mottola (MM) gravastar conjecture within the Einsteinian geometric framework. It is thought to be a promising alternative to the Black Holes (BH). Three regions make up the gravastar's structure: the interior, intermediate shell, and the exterior region. In our model, the interior core region is characterized by a pressure equal to the constant negative matter energy density. This gives rise to a constant repulsive force acting on the shell. This shell is modeled as being composed of an ultra-relativistic plasma fluid. In conformity with Zeldovich's stiff fluid conjecture, where the pressure is proportional to the energy density of the matter cancels the repulsive force exerted by the interior region. We have described the exterior region's geometry by the Schwarzschild solution with the spacetime being a vacuum. The specifications lead to a family of exact solutions for the gravastar, free of singularities possessing a physically valid features within the $(3 + 1)$ dimensional spacetime paradigm. Moreover, our discussion has covered the junction and the energy conditions in detail, highlighting their role in the production of the thin shell. We conducted a comprehensive stability analysis of our gravastar model through the study of surface redshift and speed of sound. Thus, we have successfully formulated a stable gravastar model that overcomes the singularity problem of BHs, within the context of General Relativity (GR).

Keywords Gravastar · Buchdahl metric potential · Black Holes

1 Introduction

The Schwarzschild solution has been a source of ongoing controversy with disagreements persisting over the possibility of compressing matter within the gravitational radius, as defined by $2GM$. The occurrence of super-massive compact objects with masses between $10^6 M_\odot$ and $10^9 M_\odot$ provided indications for the existence of BH like objects [1, 2]. In analyzing the thermodynamic behavior of charged Gauss–Bonnet anti de-Sitter BHs in five dimensions, employment of a topological approach treating critical points and BH states as defects in the thermodynamic parameter space can be seen in [3]. Also, a novel family of rotating BH solutions are also shown by applying the Newman–Janis algorithm to incorporate an anisotropic matter field which leads to an additional hair parameter from the negative radial pressure alongside mass, charge, and spin [4]. However, the issue that persists is whether the Schwarzschild metric offers an accurate portrayal of the internal physics. Researchers have proposed with time alternative BH scenarios that remove interior singularities [5–10]. A relatively simple model for super-massive compact objects in galactic nuclei involves a self-gravitating gas of degenerate fermions, composed of heavy sterile neutrinos [11–14]. Nevertheless, this scenario is insufficient to account for the entire mass range of super-massive BH candidates using a sterile neutrino species [15]. A novel proposal has recently been put forward, which draws

✉ Meghanil Sinha
meghanil1729@gmail.com

Mahesh Kumar
mk925726@gmail.com

S. Surendra Singh
ssuren.mu@gmail.com

Javlon Rayimbaev
javlon@astrin.uz

Inomjon Ibragimov
i.ibragimov@kiut.uz

[1] Department of Mathematics, National Institute of Technology Manipur, Imphal 795004, India

[2] New Uzbekistan University, 100007 Tashkent, Uzbekistan

[3] Urgench State University, 221100 Urgench, Uzbekistan

[4] Kimyo International University, 100121 Tashkent, Uzbekistan

Published online: 26 September 2025

analogies from condensed matter systems where effectively GR manifests as an emergent property [6]. It was proposed that the vanishing of the lapse function at a particular sphere indicated a quantum phase transition, followed by an increase in the lapse function for $r < 2GM$. The authors assumed a vacuum condensate in the interior governed by a de-Sitter spacetime, with an EoS $p = -\rho$, to satisfy the requirement of negative pressure [6].

Building on this concept, MM later introduced the idea of gravitational vacuum condensate star or gravastar where the event horizon is replaced by a shell of stiff matter at the surface, located at $r = 2GM$ [8]. They originally proposed the idea of gravastars, a theoretical framework for gravitational vacuum condensate stars as an alternative to traditional BH theory. It is commonly assumed that any variety of repulsive, non-thermal pressure from degenerate elementary particles can be overcome. Through further development of the Bose–Einstein condensation, MM's work introduced a new solution, the model they developed consisted of a cold, dark and compact object with a de-Sitter condensate phase in its interior and a Schwarzschild metric describing its exterior. A thin shell of finite thickness consisting of stiff fluid exhibiting the EoS $p = \rho$ was postulated in between the two spacetimes. The new solution was shown to be stable from a thermodynamic perspective, avoiding the information paradox that plagues BHs. The gravastar can be thought of as a three-layered structure with different EoSs describing the behavior of matter in each region as

I Interior $[0 \leq r < r_1] \longrightarrow p = -\rho.$

II Intermediate thin shell $[r_1 \leq r \leq r_2] \longrightarrow p = \rho.$

III Exterior $[r_2 < r] \longrightarrow p = \rho = 0.$

A considerable body of research on gravastars, spanning various mathematical and physical aspects, can be found in the existing literature [16–24]. A significant portion of these studies have been framed within the theoretical foundations of Einstein's GR. Researchers have examined whether gravastars are stable or not using the mathematical framework of Israel thin shell formalism [16, 18, 25]. The dynamic stability of the gravastars characterized by thin shell has also been the subject investigation lately [16, 27]. Gravastar models were built joining an interior de-Sitter or anti de-sitter region to an exterior spacetime resembling a Schwarzschild anti de-Sitter or Reissner–Nordström BH [18]. In the theoretical setting of Reissner–Nordström spacetime, two models of gravastars were introduced and the role and influence of charge on the stabile gravastar configurations were initiated [26]. Thin shell gravastars with electromagnetic fields were analyzed during revealing their entropy characteristics [23]. A theoretical model of a gravastar was developed, incorporating phantom energy to examine its evolutionary dynamics [28]. Gravastars were studied with continuous pressure via the Chandrasekhar approach, and an EoS was derived for the static configuration [29]. A theoretical framework for thin shell gravastars in $(2 + 1)$ dimensional framework was proposed, and their entropy, length, and energy conditions were systematically analyzed [30]. A study examined the physical characteristics of non-commutative gravastar solutions, with emphasis on the stability of the transitional layer configuration [32]. It was demonstrated that the thin shell behaves stably near the event horizon. A perturbative analysis of non-commutative thin shell gravastars was performed, employing radial perturbations to elucidate stable regions [31]. Recent research focused on thin shell gravastars, constructed by matching interior de-Sitter spacetime with exterior Bardeen and Bardeen-de-Sitter BH spacetimes [33]. It was revealed that with the increase of the cosmological constant leads to larger stable regions, whereas increasing the exterior spacetime charge has the opposite effect.

Several modified theories of gravitational framework have been proposed with time to account for the observed acceleration of the Universe, viz., $f(T), f(Q), f(R,T), f(Q,T), f(R,L_m,T)$, and others also with the modifications involve altering either the geometrical sector or the matter-energy content of the Einstein field equations (EFE). Since its introduction, gravastar model has been analyzed and explored in modified theories of gravity providing new insights into its properties [34–38]. Also, a comprehensive analysis of the gravastar model has been performed, incorporating various conditions to examine its viability and implications. In a study, researchers constructed a cylindrical, charged gravastar-like structure investigated its behavior in modified gravity theory [39]. A similar study analyzed the stability of gravastars in cylindrical spacetime under linear perturbations, exploring the effects of equilibrium conditions and charge variations [40]. A paper presented a model of charged gravastars based on de-Sitter– Reissner–Nordström spacetime, highlighting the importance of charge in ensuring the stability of the gravastar and indicated that when the charge exceeds a critical value, the gravastar's configuration is disrupted resulting in a collapse to a BH [41]. Physicists investigated the viability of charged gravastars in higher-dimensional theories concluding that the incorporation of extra dimensions is not supported by fundamental physical principles [42]. A investigation was carried out for the charged gravastar model in a spherically symmetric spacetime background, employing modified gravity framework to elucidate stability conditions [43]. A stable charged gravastar model has been demonstrated to exist also in cylindrically symmetric spacetime [44]. A gravastar model was formulated in the context of GR, specifically in $(2 + 1)$ dimensional spacetime

and also a gravastar model featuring a charged interior was constructed admitting conformal motion with an exterior spacetime given by Reissner–Nordström line element [45].

In the light of the previous findings, we investigate the behavior of a gravastar model within the framework of $(3+1)$ dimensional spherically symmetric spacetime utilizing the Buchdahl metric potential in this paper. Our gravastar model consists of three regions namely the interior, shell, and the exterior following the MM conjecture. To determine the metric potential of the radial component, we have taken the physically, feasible, singularity-free Buchdahl metric potential for the g_{tt} in the interior and also in the shell. Using this metric with an ideal fluid distribution, we have examined different features of the interior and the shell which is modeled to be consisting of ultra-relativistic stiff fluid. The reason behind adoption of this type of metric function is that this metric potential is completely free from any singularity and shows a regular behavior throughout the gravastar. We have also calculated different properties of the shell, which have shown the physical acceptability of the gravastar under our present study. The exterior region is defined by the Schwarzschild metric, which characterizes the external vacuum spacetime model. The proposed model retains the physical role of the interior with repulsive characteristics that can prevent singularity formation and this choice ensures that the interior solution remains physically reasonable and consistent with GR constraints. The thin shell, which is modeled with a stiff fluid, is consistent with the original MM gravastar construction. The exterior geometry described by the Schwarzschild metric ensures asymptotic flatness and consistency with astrophysical BH observations. The form for the Buchdahl metric function which we have assumed here can be found in the works of [46, 47]. We can see for the case of anisotropy also, where this Buchdahl metric function has been utilized to analyze the stellar structures. By employing two specific anisotropic stellar solutions, modified compactness bounds that depend explicitly on anisotropy parameters have been derived [48]. In another study, we can see how the authors have extended the classical Buchdahl bound for the maximum compactness limit for a stable, spherically symmetric object in GR to include both electromagnetic charge and modifications from modified gravitational gravity [49]. Hence, our analysis incorporating this metric function yields a new set of solutions for the three separate regions accompanied by each of its corresponding EoS. For the purpose of assessing the stability of the model, we performed a detailed analysis of the surface redshift and speed of sound which serve as the key indicators of stability. Furthermore, our analysis included the study of junction conditions that govern the thin shell creation. A key feature of this function is that the metric potential and its radial derivative are analytic and non-singular at the stellar origin, $r = 0$, and by employing this approach, we can systematically construct the non-singular solutions in $(3+1)$ dimensional spacetime.

The organization of this paper is outlined as follows: We begin with a concise introduction to the gravastar model in Sect. 1. In Sect. 2, we lay the mathematical foundation for the gravastar model. Section 3 presents a detailed analysis of the interior region of the gravastar yielding non-singular solutions. Sections 4 and 5 are devoted to the shell region and the exterior spacetimes respectively. Section 6 explores the junction conditions, which enable the continuous matching of the interior and exterior spacetime geometries across a smooth hypersurface. We assess the stability of our proposed gravastar model in Sect. 7. Section 8 provides an in-depth examination of the gravastar's physical attributes, including proper length, energy, and entropy as a function of shell thickness. We have discussed the necessary energy conditions in Sect. 9, and finally, we conclude our paper with a summary of our main results in Sect. 10.

2 Mathematical formalism of the field equations

We adopt a static, spherically symmetric metric whose line element is specified by the expression below

$$ds^2 = e^{\psi(r)}dt^2 - e^{\Sigma(r)}dr^2 - r^2(d\theta^2 + \sin^2\theta d\phi^2), \tag{1}$$

where ψ and Σ are functions of the radial parameter. We begin with the Einstein–Hilbert action, incorporating the coupling to matter fields is provided by

$$I = \int (R + 2\kappa L_f)\sqrt{-g}d^4x. \tag{2}$$

The principle of least action, applied to this action leads to the formulation of the Einstein equations. Concerning the gravitational field we choose the Lagrangian to be R, the Ricci scalar where $R = g_{mn}R^{mn}$. L_f represents the Lagrangian for matter and other fields while $\kappa = \frac{8\pi\mathbb{G}}{c^4}$ is the Einstein's gravitational constant. We denote $\mathbb{G}$ as the Universal gravitational constant, and c as the fundamental constant representing the light speed in empty space. Now, we consider $\mathbb{G} = c = 1$ in the relativistic units in our work, which has been used all through in the further analysis. Variation of I w.r.t g_{mn} leads to the field equation

$$R_{mn} - \frac{1}{2}g_{mn}R = -8\pi T_{mn}. \tag{3}$$

For the matter field, we consider the energy momentum tensor T_{mn} to have exhibiting a perfect fluid nature

$$T_{mn} = (\rho + p)u_m u_n - p g_{mn}, \tag{4}$$

where we have ρ as the energy density, p as the isotropic pressure with u_m the four-velocity vector of the fluid. Equation (1) leads to the formulation of EFE as

$$e^{-\Sigma}\left(\frac{\Sigma'}{r}-\frac{1}{r^2}\right)+\frac{1}{r^2}=8\pi\rho \tag{5}$$

$$e^{-\Sigma}\left(\frac{\psi'}{r}+\frac{1}{r^2}\right)-\frac{1}{r^2}=8\pi p \tag{6}$$

$$\frac{e^{-\Sigma}}{4r}\left[(2\psi''+\psi'^2-\psi'\Sigma')r-2(\Sigma'-\psi')\right]=8\pi p, \tag{7}$$

where ($'$) symbol indicates the derivative w.r.t r. We consider a non-singular metric potential for the g_{tt} component for gravastar model in $(3+1)$ dimensional framework [50]. As a specific choice, we adopt here the Buchdahl metric potential, whose expression takes the form as

$$e^{\psi(r)}=\frac{G(Hr^2+1)}{G+Hr^2} \qquad 0<G<1, \tag{8}$$

where G denotes an arbitrary dimensionless constant H function of r indicating a de-Sitter metric for the interior spacetime. At the stellar origin, both the metric function and its radial derivative are finite and well behaved at the origin, as demanded

$$e^{\psi(0)}=1, \qquad \partial_r e^{\psi(r)}|_{r=0}=0. \tag{9}$$

By incorporating the above condition into the equations (5)–(7), we obtain the resulting equations as

$$8\pi\rho=e^{-\Sigma}\left(\frac{\Sigma'}{r}-\frac{1}{r^2}\right)+\frac{1}{r^2} \tag{10}$$

$$8\pi p=e^{-\Sigma}\left(-\frac{2GH(1+Hr^2)}{(G+Hr^2)^2}+\frac{2GH}{G+Hr^2}+\frac{1}{r^2}\right)-\frac{1}{r^2} \tag{11}$$

$$\begin{aligned}8\pi p=&\frac{e^{-\Sigma}}{2r\left(G+Hr^2\right)^4}\times\Big(H^4\Sigma' r^8+GH^3r^4(-12+2r+3\Sigma' r^2)\\&GH^2r^2(-8+2r+4(3H+\Sigma')r^2-2Hr^3+H\Sigma' r^4)\\&G^3H(4+2r+(8H+3\Sigma')r^2+2H\Sigma' r^4)\\&G^4(\Sigma'-2H^2r^3+H(-4-2r+\Sigma' r^2))\Big).\end{aligned} \tag{12}$$

In $(3+1)$ dimensional framework, conservation of the stress-energy tensor results in

$$\frac{1}{2}(\rho+p)\psi'+p'=0. \tag{13}$$

The gravastar is a three-layered structure, with each layer obeying a distinct EoS as specified by

- Interior (Region I) : $0\le r<r_1, \quad p=-\rho.$
- Shell (Region II) : $r_1<r<r_2, \quad p=\rho.$
- Exterior (Region III) : $r_2<r, \quad p=\rho=0.$

3 Interior region

Inserting the EoS for the interior region into Eq. (13) results in

$$p=-\rho=-\rho_\theta; \tag{14}$$

ρ_θ characterizes the constant matter density. Clearly, the pressure also remains constant here. The analysis reveals a homogeneous and isotropic distribution of pressure and density within the gravastar's interior. Applying the condition from Eq. (14) into Eq. (10) gives us

$$e^{-\Sigma}=-\frac{8\pi\rho_\theta r^2}{3}+1+\frac{B}{r}, \tag{15}$$

where B indicates the constant of integration. The regularity condition at $r=0$ necessitates setting $B=0$, thereby obtaining

$$e^{-\Sigma}=\frac{3-8\pi\rho_\theta r^2}{3}. \tag{16}$$

We require $3-8\pi\rho_\theta r^2$ to be non-zero to avoid singular behavior. Figure 1 displays the variation of $e^{\Sigma(r)}$ in the interior section. As evident, the solution exhibits smooth behavior and absence of singularities at the center. The active gravitational mass for the interior region of our stellar model can be computed as

$$\check{M}=\int_0^{r_1=D}4\pi r^2\rho dr=\frac{4\pi D^3\rho_\theta}{3}, \tag{17}$$

where $r_1=D$ defines the internal boundary of the gravastar. Figure 2 displays the behavior of the active gravitational mass in the interior sector, where we find that as the radius grows, the active gravitational mass increases and exhibits a regular behavior.

4 Shell region

The shell formation occurs at the meeting point of two spacetime manifolds, namely, the regions marked as I and III. The shell has a negligible, yet finite thickness and all the matter of the collapsing star is confined with it. In conjunction with the cold, compact baryonic Universe, the behavior of this matter in ultra-relativistic regime is described by the stiff fluid concept, introduced by Zeldovich [51]. This fluid satisfies the EoS $p=\rho$ indicating a direct proportionality between pressure and density, which

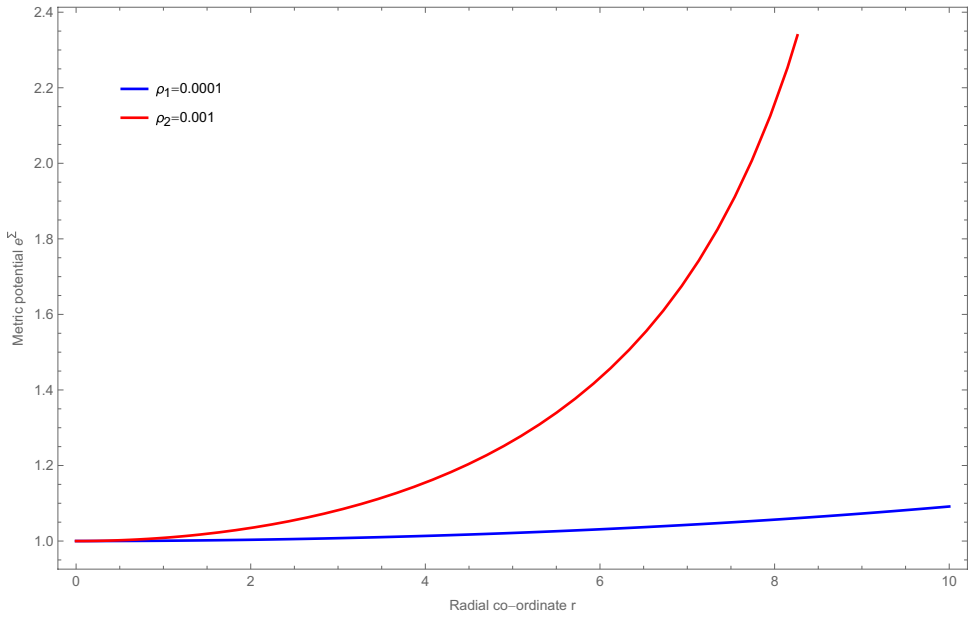

Fig. 1 Variation of $e^{\Sigma(r)}$ with respect to the radial co-ordinate for $\rho_\theta = 0.0001$ [50] and $\rho_\theta = 0.001$ [36]

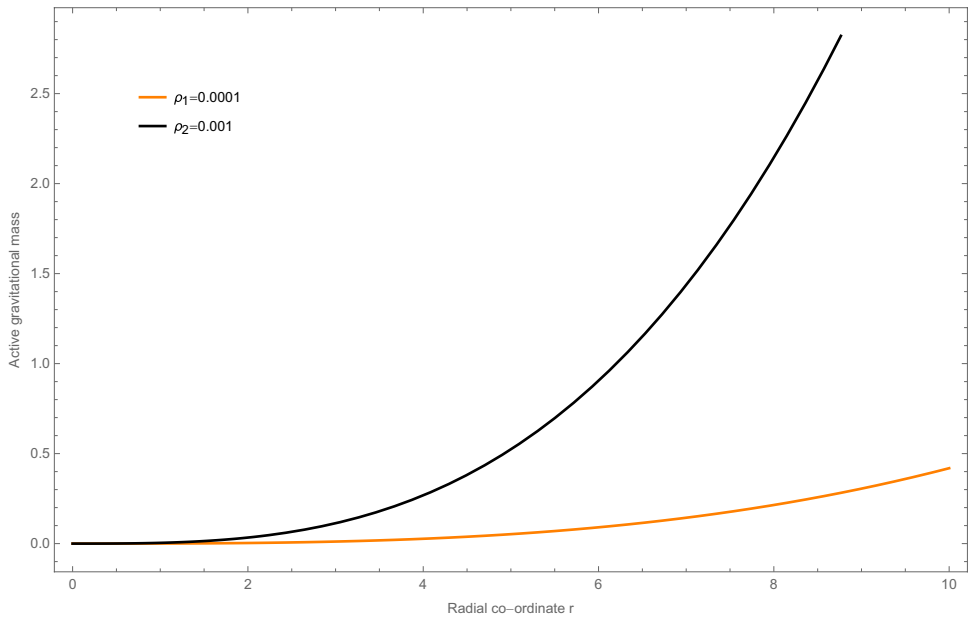

Fig. 2 Variation of the active gravitational mass with respect to the radial co-ordinate for $\rho_\theta = 0.0001$ and $\rho_\theta = 0.001$

furnishes the requisite force to counterbalance the repulsive effects coming from the inner part sustaining the system's stable equilibrium state. Researchers in cosmology and astrophysics have widely utilized this type of fluid to develop viable explanations [52, 53]. We aim to derive a mathematically consistent and satisfactory framework to understand the thin shell formation. Solving the field equations is a very hard task to be done within this non-vacuum region with the EoS $p = \rho$. By employing the thin shell approximation, we can derive an analytical solution to describe the shell's behavior. Given the shell's thinness to be very small, any r- dependent parameter can be considered to be $\ll 1$. Within the thin shell approximation, the metric function $e^{\Sigma(r)}$ can be explicitly determined by resolving Eqs. (10) and (11) as

$$e^{\Sigma(r)} = Nr^2 e^{\frac{G-G^2}{G+Hr^2}} \tag{18}$$

with N being the integration constant. The behavior of $e^{\Sigma(r)}$ has been analyzed in Fig. 3, revealing a well-behaved variation without singularities for various parameter values. A combination of the Eq. (13) and the shell's EoS enables us to compute the density and pressure of the shell as

$$\rho = p = \rho_K e^{\frac{(-1+G)G}{G+Hr^2}}, \tag{19}$$

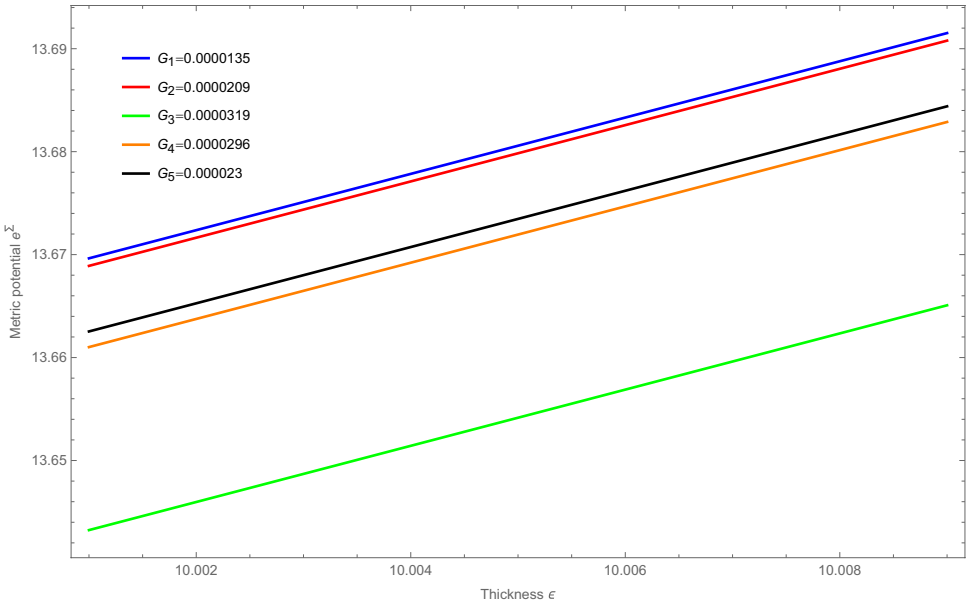

Fig. 3 Variation of $e^{\Sigma(r)}$ within the shell with respect to the thickness of the shell for $(i)PSRJ1614-2230(G=0.0000135, H=-7.455\times10^{-8}km^2)$, $(ii)4U1608-52(G=0.0000209, H=-1.1446\times10^{-7}km^2)$, $(iii)SAXJ18808.4-3658(G=0.0000319, H=-1.5664\times10^{-7}km^2)$, $(iv)4U1538-52(G=0.0000296, H=-1.4545\times10^{-7}km^2)$, and $(v)SMCX-1(G=0.000023, H=-1.154\times10^{-7}km^2)$ [47]

where ρ_K represents the constant of integration. The density variation in Fig. 4 indicates an increase from the interior directed toward the outer boundary, which implies that the shell's compactness is greater at the external boundary interface than at the interior.

5 Exterior region

The exterior region of the gravastar is modeled as a complete vacuum, where the pressure and density are both zero

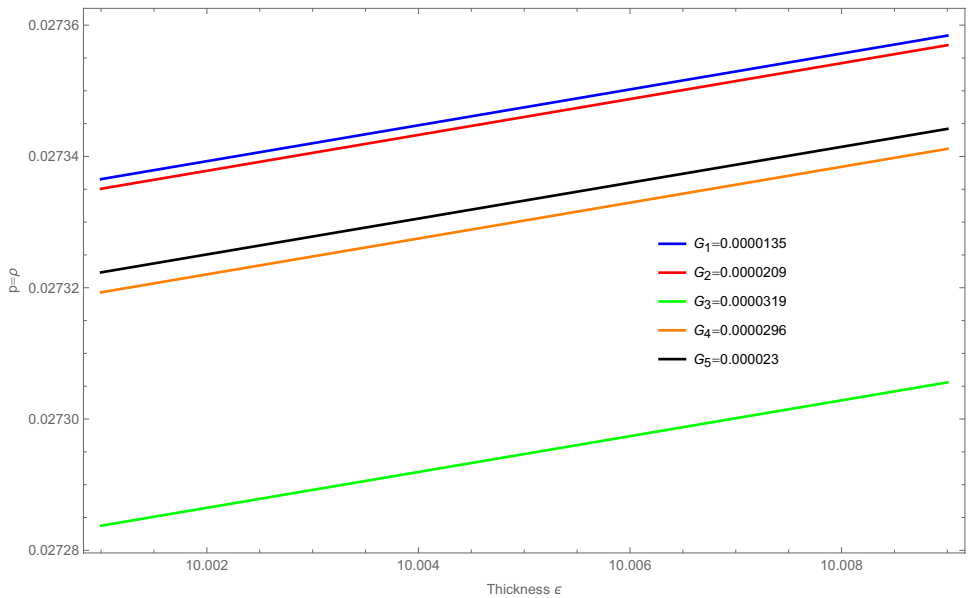

Fig. 4 Density profile of the shell is plotted versus its thickness for $(i)PSRJ1614-2230(G=0.0000135, H=-7.455\times10^{-8}km^2)$, $(ii)4U1608-52(G=0.0000209, H=-1.1446\times10^{-7}km^2)$, $(iii)SAXJ18808.4-3658(G=0.0000319, H=-1.5664\times10^{-7}km^2)$, $(iv)4U1538-52(G=0.0000296, H=-1.4545\times10^{-7}km^2)$, and $(v)SMCX-1(G=0.000023, H=-1.154\times10^{-7}km^2)$

($p = \rho = 0$). The corresponding spacetime metric takes the form as

$$ds^2 = \left(1 - \frac{2M}{r}\right)dt^2 - \frac{1}{\left(1 - \frac{2M}{r}\right)}dr^2 - r^2\left(d\theta^2 + \sin^\theta d\phi^2\right), \tag{20}$$

which corresponds to the Schwarzschild-type vacuum solution in $(3 + 1)$ dimensional spacetime. The parameter M corresponds to the gravastar's total mass.

6 Junction conditions

The gravastar model has three separate regions, each characterized by a unique EoS that governs its behavior. Regions (I) and (III) are separated by the thin shell. As a result, it plays a significant part in the gravastar's structure. The outcome is thus a geodetically complete manifold, featuring a surface situated matter shell. The gravastar configuration is thereby separated by a single manifold. The interior (I) and exterior (III) regions need to be smoothly matched at the junction in accordance with the primary junction constraint. While the metric co-efficients themselves are continuous at the junction, their derivatives might not be. Application of the Darmois–Israel junction condition will facilitate the computation of the surface stresses at the junction interface (S) [54–56]. As a fundamental requisite for the junction condition, regions of interior and exterior must match smoothly at the junction. To determine the potential across the thin shell, we see that the Israel junction conditions are applicable if the shell's thickness is negligible. Mathematically, this implies that the shell is a hypersurface with one dimension less than the embedding manifold. Beyond the shell, the transitioning to de-Sitter space inside is expected to occur through a quantum phase transition. In this context, the shell represents a thin boundary between two spacetimes; otherwise, a thick shell would undergo significant changes or disruptions during the phase transition. We use the junction condition here as there are two different metrics across the thin shell that match the condition along the boundary since the metric along the hypersurfaces must be continuous as well as differentiable. We can see the thin-wall formalism for vacuum bubble nucleation in gravitational theories like Brans–Dicke-type scalar-tensor gravity, where the authors have generalized the junction conditions to include the Brans–Dicke scalar and have recast the resulting wall equation into a mechanical form with an effective potential [57]. This framework successfully provides a clear prescription to derive the junction equation across the bubble wall and also a practical route to compute the effective potential that governs bubble dynamics and the Euclidean bounce relevant for nucleation rates. Also, the development for the junction conditions for this Brans–Dicke–type gravity in the thin-wall limit can be seen in the works of [58], where the derived equation of motion, rearranged into a form with an effective potential, serves as a powerful tool for analyzing dynamical regimes like expansion or collapse of false vacuum bubbles. The Lanczos equation provides an explicit representation of the intrinsic surface energy tensor $S_{\alpha\beta}$ [59–62]

$$S^\alpha_\beta = -\frac{1}{8\pi}\left(\kappa^\alpha_\beta - \delta^\alpha_\beta \kappa^K_K\right). \tag{21}$$

Here, $\kappa_{\alpha\beta} = K^+_{\alpha\beta} - K^-_{\alpha\beta}$, the $(+)$ sign corresponds to the exterior surface and $(-)$ sign corresponds to the interior interface. The second fundamental form is formulated as

$$K^\pm_{\alpha\beta} = -n^\pm_\pi\left[\frac{\partial^2 x_\pi}{\partial\xi^\alpha\partial\xi^\beta} + \Gamma^\pi_{ij}\frac{\partial x^i \partial x^j}{\partial\xi^\alpha\partial\xi^\beta}\right]\Big|_S. \tag{22}$$

In this context, ξ^α denotes the extrinsic co-ordinates on the shell, $n^\pm_\pi$ the unit normals on the surface and for the spherically, symmetric static metric

$$ds^2 = h(r)dt^2 - h(r)^{-1}dr^2 - r^2\left(d\theta^2 + \sin^\theta d\phi^2\right) \tag{23}$$

and an explicit expression for $n^\pm_\pi$ is

$$n^\pm_\pi = \pm\left|g^{ij}\frac{\partial h}{\partial x^i}\frac{\partial h}{\partial x^j}\right|^{-\frac{1}{2}}\frac{\partial h}{\partial x^\pi}. \tag{24}$$

Here, $n^\upsilon n_\upsilon = 1$. By applying the Lanczos equation, the surface stress-energy tensor at the interface boundary can be formulated as $S_{\alpha\beta} = \text{diag}\,(\Theta, -\Xi, -\Xi, -\Xi)$. In this expression, Θ represents the surface energy density and Ξ the surface pressure. The definition of these parameters are determined as

$$\Theta = -\frac{1}{4\pi D}\left(\sqrt{h}\right)^+_- \tag{25}$$

and

$$\Xi = -\frac{\Theta}{2} + \frac{1}{16\pi}\left(\frac{h'}{\sqrt{h}}\right)^+_-. \tag{26}$$

The surface energy density and surface pressure can be explicitly determined from the above equations as

$$\Theta = -\frac{1}{4\pi D}\left(\sqrt{1 - \frac{2M}{D}} - \sqrt{\frac{3 - 8\pi\rho_\theta D^2}{3}}\right) \tag{27}$$

and

$$\Xi = \frac{1}{8\pi D}\left[\frac{1 - \frac{M}{D}}{\sqrt{1 - \frac{2M}{D}}} - \frac{3 - 16\pi\rho_\theta D^2}{\sqrt{9 - 24\pi\rho_\theta D^2}}\right]. \tag{28}$$

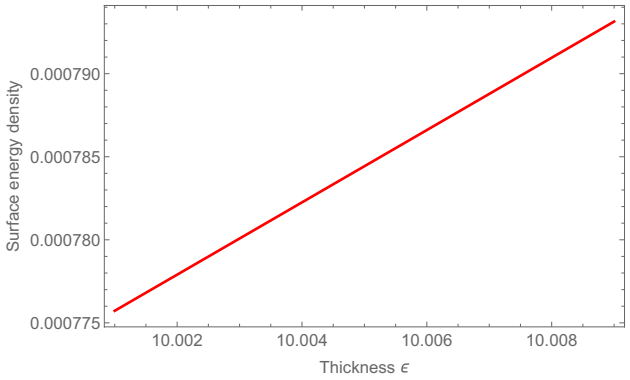

Fig. 5 The surface energy density is plotted with respect to the thickness parameter ϵ(km) for $M = 3.388M_{\odot}$ [63]

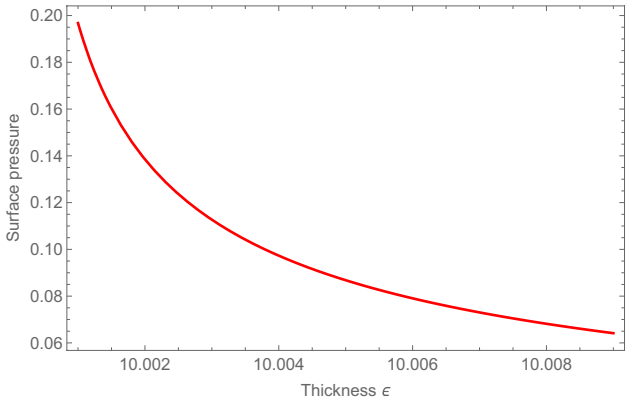

Fig. 6 The surface pressure is plotted with respect to the thickness parameter ϵ(km) for $M = 3.388M_{\odot}$ and $\rho_{\theta} = 0.0001$

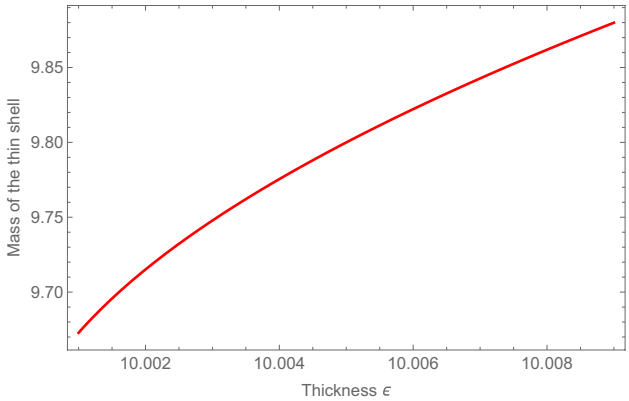

Fig. 7 A plot of the thin shell mass M^{Shell} versus the thickness parameter ϵ(km) is presented for $M = 3.388M_{\odot}$, $\rho_{\theta} = 0.0001$

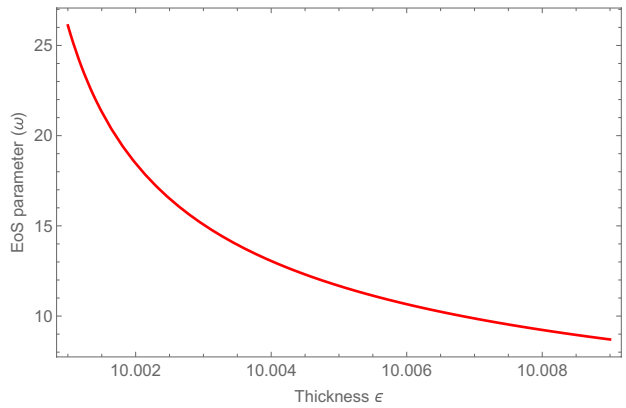

Fig. 8 The EoS parameter (ω) is plotted with respect to thickness parameter ϵ(km) for $M = 3.388M_{\odot}$, $\rho_{\theta} = 0.0001$

Figures 5 and 6 show how the surface energy density and surface pressure vary. Results show that the parameters are uniformly positive within the shell. This outcome implies that the null energy condition has been satisfied allowing the shell formation. As we move toward the outer boundary, we can see that the surface energy density parameters increase, while the surface pressure decreases. With Eq. (27), the mass of the thin shell is found to be

$$M^{Shell} = 4\pi D^2\Theta = \left[\sqrt{D^2 - \frac{8}{3}\pi\rho_{\theta}D^4}\right]. \tag{29}$$

The results for the thin shell mass variation are visualized in Fig. 7. The plot shows an increase toward the outer boundary. We derive the total mass of the gravastar using the above Eq. (29) as

$$M = \frac{4\pi\rho_{\theta}D^2}{3} + M^{Shell}\sqrt{(1 - \frac{8}{3}\pi\rho_{\theta}D^2)} - \frac{(M^{Shell})^2}{2D}. \tag{30}$$

The EoS parameter (ω) is described by

$$\omega(D) = \frac{\Xi(D)}{\Theta(D)}; \tag{31}$$

the EoS parameter calculated from Eqs. (27) and (28) results in

$$\omega(D) = \frac{\left(\frac{1-\frac{M}{D}}{\sqrt{1-\frac{2M}{D}}} - \frac{3-16\pi\rho_{\theta}D^2}{\sqrt{9-24\pi\rho_{\theta}D^2}}\right)}{2\left(\sqrt{1-\frac{8\pi\rho_{\theta}D^2}{3}} - \sqrt{1-\frac{2M}{D}}\right)}. \tag{32}$$

Evidently from Fig. 8, we can see that $\omega(D)$ decreases as it approaches the external boundary with increasing shell thickness.

7 Stability analysis

The stability of our star model has been assessed in this section via two separate methods: $< i >$ surface redshift and $< ii >$ speed of sound analysis. The methods used are obtained below.

7.1 Surface redshift

The study of surface redshift is a key source of insight into evaluating the stability and detectability of gravastars. The surface gravitational redshift is characterized by $Z_S = \frac{\Delta\lambda}{\lambda_e} = \frac{\lambda_o}{\lambda_e}$, $\Delta\lambda$ embodies the fractional difference in wavelengths between the emitted λ_e and observed signals λ_o. It was asserted that the surface redshift of a static, isotropic perfect fluid cannot exceed a value of 2 [64–66]. For anisotropic fluid distribution, the surface redshift limit has been proposed to be as high as 3.84 [67]. Studies also revealed that, for isotropic fluid distributions without a cosmological constant $Z_S \leq 2$ [68]. It was again shown that, considering the cosmological constant, the surface redshift (Z_S) of an anisotropic star is bounded above by 5 [66]. To determine the surface redshift, we have utilized the following equation as:

$$Z_S = -1 + \mid g_{tt} \mid^{-\frac{1}{2}} . \tag{33}$$

Consequently, we obtain the surface redshift as

$$Z_S = -1 + \sqrt{\frac{G + Hr^2}{G(Hr^2 + 1)}}. \tag{34}$$

We have graphed the surface redhsift variation in Fig. 9. As seen in the figure, the value of Z_S remains within 1 across the whole thin shell for varying values of the parameters. Based on our analysis, our gravastar model can be deemed stable and physically acceptable.

7.2 Speed of sound analysis

The stability analysis of gravastar can be facilitated by examining the properties and behavior of η. Here, η is an effective parameter that corresponds to the square of the sound speed, i.e., $\eta = v_s^2$ [69, 70]. A stable system requires η to satisfy the condition $0 < \eta \leq 1$. Clearly, the speed of sound should not exceed the speed of light. However, this restriction may not be satisfied on the surface layer. The square of the speed of sound is defined by [71]

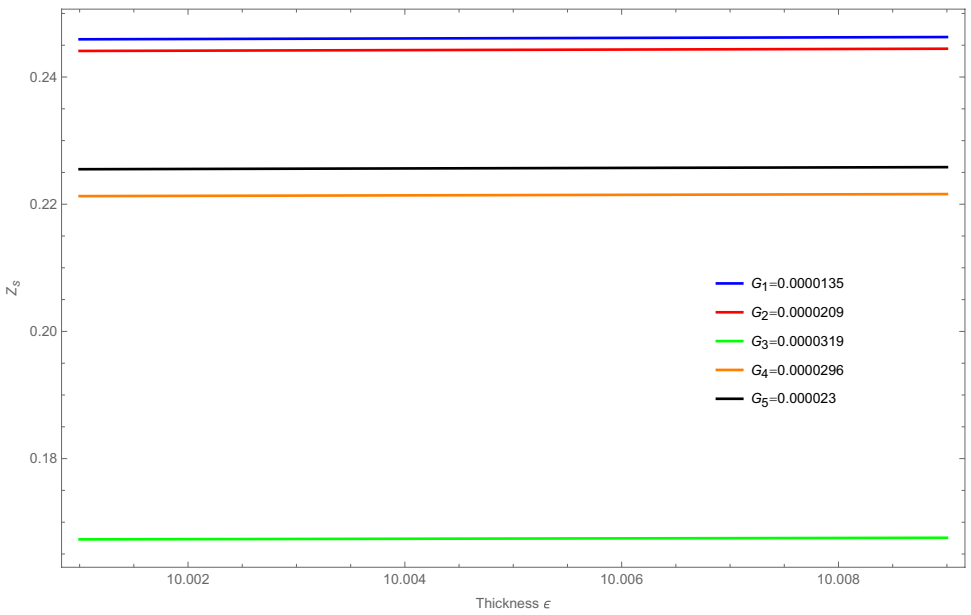

Fig. 9 Z_S is plotted with respect to thickness parameter ϵ(km) for $(i)G = 0.0000135, H = -7.455 \times 10^{-8} km^2$, $(ii)G = 0.0000209, H = -1.1446 \times 10^{-7} km^2$, $(iii)G = 0.0000319, H = -1.5664 \times 10^{-7} km^2$, and $(iv)G = 0.0000296, H = -1.4545 \times 10^{-7} km^2$, $(v)G = 0.000023, H = -1.154 \times 10^{-7} km^2$

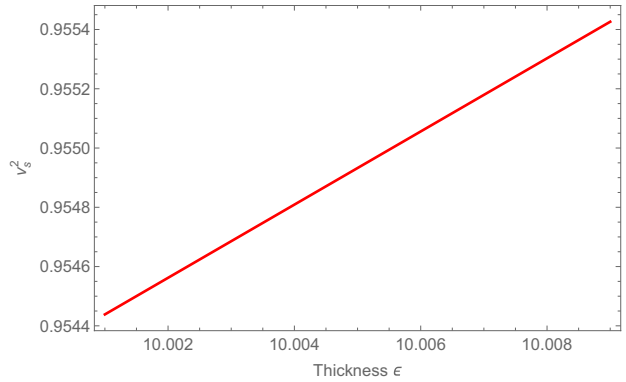

Fig. 10 The change of $\eta = v_s^2$ is plotted with respect to the thickness parameter ϵ(km) for $M = 3.388 M_{\odot}$, $\rho_\theta = 0.0001$

$$\eta = v_s^2 = \frac{\Xi'(D)}{\Theta'(D)}, \tag{35}$$

where the prime signifies the derivative with respect to the radial co-ordinate. Equations (27) and (28) yield

$$\eta = v_s^2 = \frac{\frac{M}{D^2\sqrt{1-\frac{2M}{D}}} - \frac{M(1-\frac{M}{D})}{D^2(1-\frac{2M}{D})^{\frac{3}{2}}} + \frac{32D\pi\rho_\theta}{\sqrt{9-24\pi D^2\rho_\theta}} - \frac{24\pi D\rho_\theta(3-16D^2\pi\rho_\theta)}{(9-24D^2\pi\rho_\theta)^{\frac{3}{2}}}}{2\left(-\frac{M}{D^2\sqrt{1-\frac{2M}{D}}} - \frac{8D\pi\rho_\theta}{3\sqrt{1-\frac{8}{3}D^2\pi\rho_\theta}}\right)}. \tag{36}$$

Due to complexity of η's mathematical expression, we focus on its graphical representation. As illustrated from Fig. 10, the effective parameter η is observed to satisfy $0 < \eta \leq 1$ across the entire shell region. The positive sign of η as depicted from the figure ensures the model's stability [71].

8 Physical aspects of parameters of gravastar

Next, we investigate the properties of the gravastar's physical characteristics, including proper length, energy, and entropy within the shell.

8.1 Proper length of the shell

With the radius at the interior edge being $r = D$ and that of the outer edge being $r = D + \epsilon$, ϵ indicates the shell's dimensional thickness which is deemed to be extremely small (i.e., $\epsilon \ll 1$). Hence, the two boundaries of the shin shell

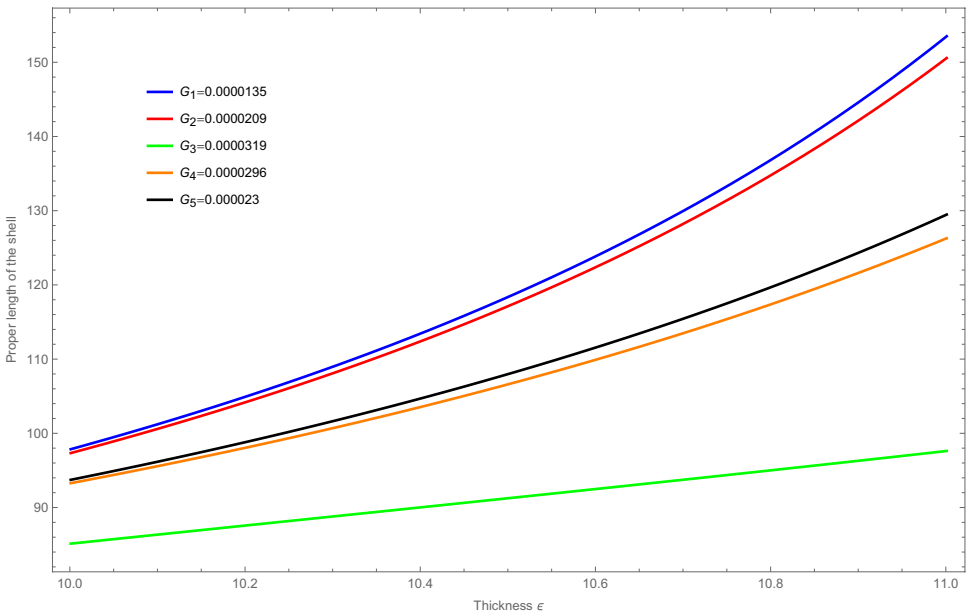

Fig. 11 A plot of the proper length of the shell versus the shell's thickness ϵ(km) for $(i) G = 0.0000135, H = -7.455 \times 10^{-8} km^2$, $(ii) G = 0.0000209, H = -1.1446 \times 10^{-7} km^2$, $(iii) G = 0.0000319, H = -1.5664 \times 10^{-7} km^2$, $(iv) G = 0.0000296, H = -1.4545 \times 10^{-7} km^2$, and $(v) G = 0.000023, H = -1.154 \times 10^{-7} km^2$

region enclose the stiff fluid in the gravastar configuration. A mathematical representation of the shell' proper length is provided as

$$\acute{l} = \int_D^{D+\epsilon} \frac{1}{\sqrt{e^{-\Sigma}}} dr = \int_D^{D+\epsilon} \sqrt{e^{\Sigma}} dr. \tag{37}$$

From Eq. (18), we derive the proper length of the shell as

$$\acute{l} = \Big[\frac{G\sqrt{e^{-\frac{(-1+G)G}{G+Hr^2}}} Nr^2}{2Hr} + \frac{G\sqrt{e^{-\frac{(-1+G)G}{G+Hr^2}}} Nr^2(2Hr^2 + e^{\frac{(-1+G)G}{2(G+Hr^2)}}(-1+G)GExpIntegralEi[-\frac{(-1+G)G}{2(G+Hr^2)}])}{4Hr} \Big]_D^{D+\epsilon}, \tag{38}$$

where $ExpIntegralEi[x]$ is the exponential integral function $Ei[x]$. A visual inspection of Fig. 11 reveals a monotonic increase in the proper length of the shell with its thickness [34, 36, 38].

8.2 Energy content within the shell

The EoS $p = -\rho$ in the interior region indicates a domain with negative energy implying a repulsive core. However, to find the energy within the shell, we will employ

$$\tilde{E} = \int_D^{D+\epsilon} 4\pi r^2 \rho dr. \tag{39}$$

With the matter density within the shell given by Eq. (19), it can be found out. We utilize a Taylor series expansion and neglect the higher order terms to simplify the expression as (since the shell is very thin)

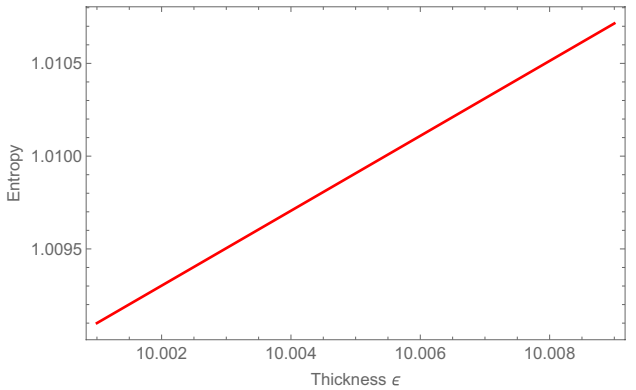

Fig. 13 A plot of the entropy of the shell versus the shell's thickness ϵ (km) for $N = 0.05$, $\rho_K = 1$ and $\epsilon = 0.0001$

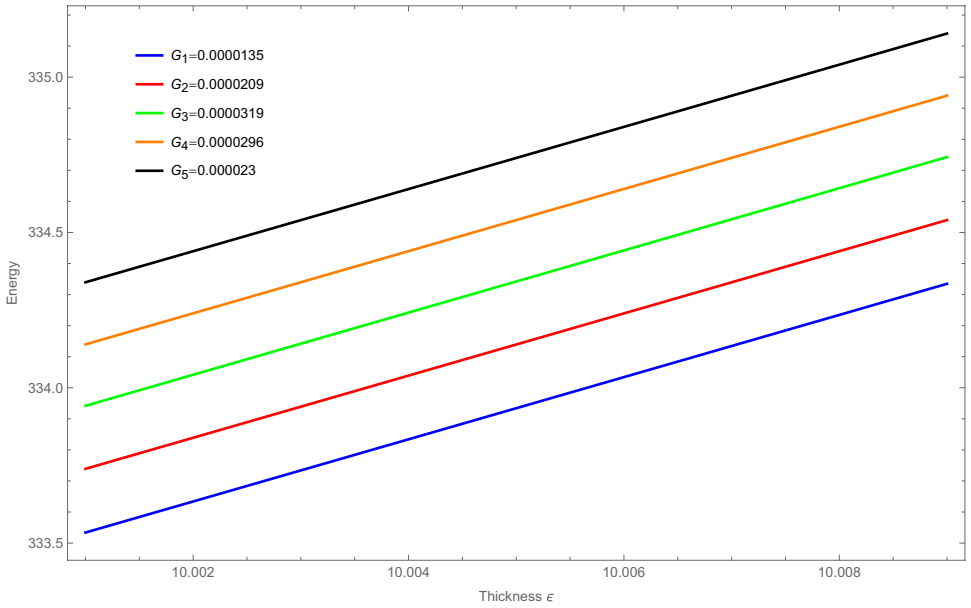

Fig. 12 A plot of the energy content within the shell versus the shell's thickness ϵ(km) for $(i)G = 0.0000135, H = -7.455 \times 10^{-8} km^2$, $(ii)G = 0.0000209, H = -1.1446 \times 10^{-7} km^2$, $(iii)G = 0.0000319, H = -1.5664 \times 10^{-7} km^2$, $(iv)G = 0.0000296, H = -1.4545 \times 10^{-7} km^2$, and $(v)G = 0.000023, H = -1.154 \times 10^{-7} km^2$

$$\tilde{E} = 4\pi\rho_K\Big[\frac{(-1+G)Gr}{H} + \frac{r^3}{3} - \frac{(-1+G)G^{\frac{3}{2}}\arctan[\frac{\sqrt{H}r}{\sqrt{G}}]}{H^{\frac{3}{2}}}\Big]_D^{D+\epsilon}. \tag{40}$$

The shell's enclosed energy is displayed graphically in Fig. 12. Our investigation demonstrates an increase in the energy content confined to the shell with respect to the thickness. The energy and matter density fluctuations exhibit similar patterns. Our findings are consistent with the prerequisite that the shell's energy increases as the radial distance increases [34, 36].

8.3 Entropy of the shell

Entropy reflects the randomness or disorderliness of the stellar system. Evidently from the review of the existing literature, we can see that the gravastar interior has zero entropy density. However, the entropy of the thin shell is described by the relation as

$$\hat{S} = 4\pi\int_D^{D+\epsilon} s(r)r^2\sqrt{e^{\Sigma(r)}}dr, \tag{41}$$

where $s(r)$ denotes the entropy density at temperature $T(r)$ by

$$\hat{S} = \frac{\beta^2 k_B^2 T(r)}{4\pi\hbar^2} = \beta(\frac{k_B}{\hbar})\sqrt{\frac{p(r)}{2\pi}} \tag{42}$$

with β as a dimensionless constant. Consequently, the entropy within the shell is formulated as

$$\hat{S} = \frac{4\pi\beta k_B}{\hbar\sqrt{2\pi}}\int_D^{D+\epsilon} r^2\sqrt{pe^{\Sigma}}dr. \tag{43}$$

In this context, we use the Planckian units $k_B = \hbar = 1$. Here, the thin shell approximation has been adopted to calculate the system's entropy. Discarding the higher order terms of the thickness parameter, we can find the entropy inside the shell to be

$$\hat{S} \approx 2\sqrt{2}\sqrt{\pi}\beta(N\rho_K)^{\frac{1}{2}}\epsilon D^2. \tag{44}$$

Our obtained results demonstrate that the entropy distribution in the shell is proportional to its thickness in the proposed gravastar model. The graphical representation of entropic characteristic of the shell is depicted in Fig. 13 with respect to the thickness. The graph demonstrates that the entropy within the shell grows with increasing shell thickness. A necessary condition for the stability in a gravastar model features that the entropy should attain its maximum value at the surface [36, 71].

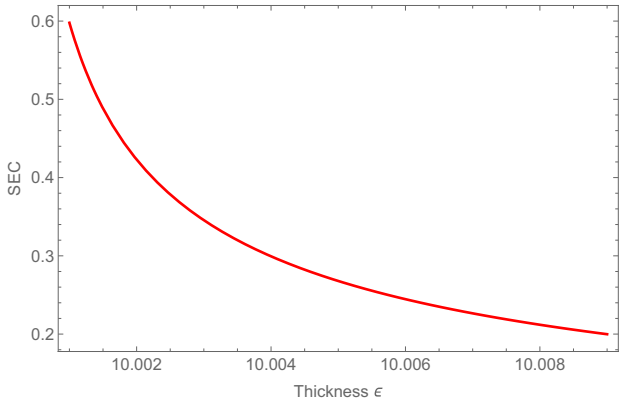

Fig. 15 A plot of SEC versus the shell's thickness ϵ(km) for $M = 3.388M_{\odot}$, $\rho_\theta = 0.0001$

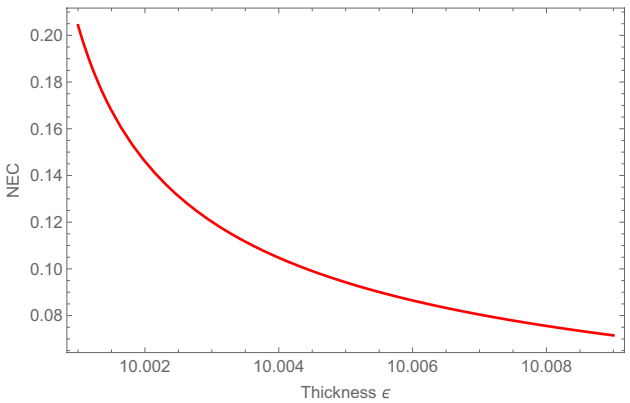

Fig. 14 A plot of NEC versus the shell's thickness ϵ(km) for $M = 3.388M_{\odot}$, $\rho_\theta = 0.0001$

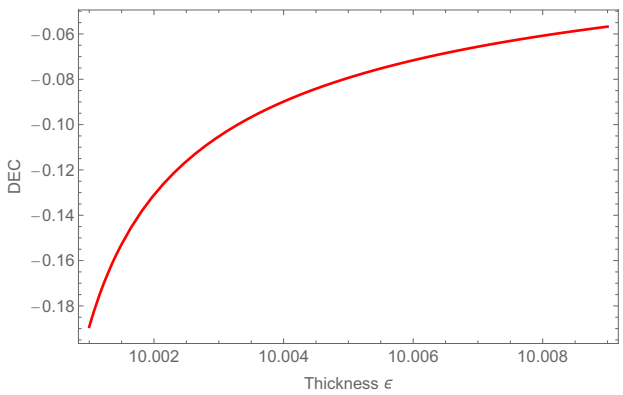

Fig. 16 A plot of DEC versus the shell's thickness ϵ(km) for $M = 3.388M_{\odot}$, $\rho_\theta = 0.0001$

9 Energy conditions

For a geometric structure to be physically viable, it must adhere to certain constraints known as energy conditions. In GR, the energy conditions are given by

(*i*) Null energy condition (NEC): $\Theta + \Xi > 0$.

(*ii*) Weak energy condition (WEC): $\Theta > 0, \Theta + \Xi > 0$.

(*iii*) Strong energy condition (SEC): $\Theta + \Xi > 0, \Theta + 3\Xi > 0$.

(*iv*) Dominant energy condition (DEC): $\Theta > 0, \Theta \pm \Xi > 0$.

Our investigation aims to determine is the NEC condition is satisfied, indicating the presence of ordinary or exotic matter within the shell. The plots in Figs. 14, 15, and 16 show the behavior of the energy conditions within the shell w.r.t to the shell thickness. Our results reveal that both NEC and SEC are satisfied throughout the entire shell, while DEC is violated in the process of the shell formation [36, 63].

10 Conclusion

In this manuscript, our analysis considered a spherically symmetric stellar system within GR, incorporating an isotropic fluid and the Buchdahl metric potential. We have formulated the EFEs within the context of $(3 + 1)$ dimensional spacetime with this metric potential and have proceeded to conduct an analysis of the geometry of a stable gravastar solution. The gravastar model comprises three distinct regions: the interior, the shell, and the exterior. The interior domain of the gravastar is characterized by the EoS $p = -\rho$ where we find the regular, singularity-free solutions for the gravitational mass and the metric co-efficients which are illustrated in Figs. 1 and 2. The fluid source in the shell region is subject to the EoS $p = \rho$(ultra-stiff perfect fluid). This part represents the interface between the inner and the outer regions, the intermediate region representing a thin shell with an infinitesimally shell thickness. Under the assumption of this approximation, our findings indicate an analytical solution that describes the thin shell of the model. Our results include well-behaved solutions for the metric co-efficients and pressure/matter density which are depicted in Figs. 3 and 4. With increasing thickness of the shell, the ulta-relativistic fluid's density increases, implying that the outer edge of the shell is denser than its inner regions. Our findings are consistent with [36, 44]. In the exterior region, the Schwarzschild solution corresponds to the solution for the vacuum model ($p = \rho = 0$).

The Darmois–Israel formalism has been employed to establish the matching constraints between the interior and exterior surfaces. The matching conditions have allowed us to determine the surface energy density and surface pressure. Figures 5 and 6 provide a visual representation of their behavior. Furthermore, we have derived the EoS parameter on the surface and also the mass of the thin shell and the results of our analysis are presented in Figs. 7 and 8. The figures provide a clear evidence that the surface energy density, surface pressure, EoS parameter, and the mass of the thin shell exhibit a monotonic increasing nature for the surface energy density and monotonic decreasing nature for surface pressure and EoS parameter with the increasing thickness. And also, we have obtained an expression for the total mass of the gravastar in terms of the thin shell mass.

Section 7 presents our model's stability, considering the surface redshift effects and speed of sound. The results show that our model is stable and meets the physical requirements, with Z_S and η lying within the stability region. We have also investigated the shell region's properties, including proper length, energy, and entropy for the shell. The results presented in Figs. 11, 12, and 13 show that the proper length, energy content, and entropy of the thin shell increase as the thickness of the shell increase. Moreover, Figs. 14, 15, and 16 demonstrate that NEC and SEC are satisfied throughout the entire shell, unlike the DEC which is not met for the construction of the thin shell. The outcome of our investigation suggests the presence of exotic matter within the shell [36, 63]. In conclusion, our proposed gravastar model resolves the limitations associated with the BHs, emerging as a viable alternative to the classical BH theory.

Author Contributions M.K and M.S wrote the main manuscript; S.S.S and J.R supervised the manuscript; I.I reviewed the manuscript.

Funding No funding was received to assist with the preparation of this manuscript.

Data Availability No datasets were generated or analyzed during the current study.

Declarations

Conflict of interest The authors declare no conflict of interest.

References

1. F. Melia, Nature **437**, 1105 (2005)
2. J. Kormendy, "The Stellar-Dynamical Search for Supermassive Black Holes in Galactic Nuclei", in Coevolution of Black Holes and Galaxies, proceedings of Carnegie Observatories Centennial

Symposium, Pasadena, California, 20–25 Oct 2002, Ed. L.C. Ho, (Cambridge Univ. Press, Cambridge 2004), pp 1–20. arXiv:astro-ph/0306353
3. I. Jeon, B.H. Lee, W. Lee, M. Mishra, Stability and topological nature of charged gauss-bonnet ads black holes in five dimensions. Phys. Rev. D **111**, 064006 (2025). arXiv:2407.20016 [hep-th]
4. H.C. Kim, B.H. Lee, W. Lee, Y. Lee, Rotating black holes with an anisotropic matter field. Phys. Rev. D **101**(6), 064067 (2020)
5. R.D. Viollier, D. Trautmann, G.B. Tupper, Phys. Lett. B **306**, 79 (1993)
6. C. Chapline, E. Hohlfeld, R.B. Laughlin, D.I. Santiago, Int. J. Mod. Phys. A **18**, 3587 (2003)
7. I. Dymnikova, Int. J. Mod. Phys. D **12**, 1015 (2003). [arXiv:gr-qc/0304110]
8. P.O. Mazur, E. Mottola, Proc. Natl. Acad. Sci. **111**, 9545 (2004). arXiv:gr-qc/0407075
9. F.S.N. Lobo, Stable dark energy stars. Class. Quant. Gravit. **23**(5), 1525 (2006)
10. A. DeBenedictis, D. Horvat, S. Ilijić, S. Kloster, K.S. Viswanathan, Class. Quant. Gravit. **23**, 2303 (2006)
11. N. Bilić, F. Munyaneza, R.D. Viollier, Phys. Rev. D **59**, 024003 (1999)
12. N. Bilić, R.L. Lindebaum, G.B. Tupper, R.D. Viollier, Phys. Lett. B **515**, 105 (2001)
13. F. Munyaneza, D. Tsiklauri, R.D. Viollier, Astrophys. J. **509**, L105 (1998)
14. F. Munyaneza, D. Tsiklauri, R.D. Viollier, Astrophys. J. ibid. 526, 744 (1999)
15. N. Bilic, G.B. Tupper, R.D. Viollier, "Sterile Neutrino Dark Matter in the Galaxy", in Particle Physics and the Universe, Proceedings of the 9th Adriatic Meeting, Dubrovnik, 2003, Eds. J. Trampetic and J. Wess, (Springer Proceedings in Physics 98, Berlin, 2004) pp 39–45
16. M. Visser, D.L. Wiltshire, Class. Quant. Gravit. **21**, 1135 (2004)
17. C. Cattoen, T. Faber, M. Visser, Class. Quant. Gravit. **22**, 4189 (2005)
18. B.M.N. Carter, Class. Quant. Gravit. **22**, 4551 (2005)
19. N. Bilić, G.B. Tupper, R.D. Viollier, J. Cosmol. Astropart. Phys. **02**, 013 (2006)
20. D. Horvat, S. Ilijić, Class. Quant. Gravit. **24**, 5637 (2007)
21. K.K. Nandi, Y.Z. Zhang, R.G. Cai, A. Panchenko, Phys. Rev. D **79**, 024011 (2009)
22. B.V. Turimov, B.J. Ahmedov, A.A. Abdujabbarov, Mod. Phys. Lett. A **24**, 733 (2009)
23. A.A. Usmani, F. Rahaman, S. Ray, K.K. Nandi, P.K.F. Kuhfittig, S.A. Rakib, Z. Hasan, Phys. Lett. B **701**, 388 (2011)
24. P. Bhar, Astrophys. Space Sci. **354**, 2109 (2014)
25. W. Israel, Nuovo Cim. B 44 S10 (1966) 1; Erratum-ibid B 48 (1967) 463
26. D. Horvat, S. Ilijić, A. Marunovic, Class. Quant. Gravit. **26**, 025003 (2009)
27. M. Sharif, F. Javed, Stability and dynamics of regular thin-shell gravastars. J. Exp. Theor. Phys. **132**(3), 381–393 (2021)
28. R. Chan, M.F.A. da Silva, P. Rocha, A. Wang, J. Cosmol. Astropart. Phys. **2009**, 10 (2009)
29. D. Horvat, S. Ilijic, A. Marunovic, Class. Quant. Gravit. **28**, 195008 (2011)
30. F. Rahaman, A.A. Usmani, S. Ray, S. Islam, Phys. Lett. B 707, 319 (2012); Phys. Lett. B 717, 1 (2012)
31. A. Övgün, A. Banerjee, K. Jusufi, Eur. Phys. J. C **77**, 566 (2017)
32. F.S.N. Lobo, R. Garattini, J. High Energy Phys. **12**, 065 (2013)
33. M. Sharif, F. Javed, Ann. Phys. **415**, 168124 (2020)
34. A. Das, S. Ghosh, B.K. Guha, Swapan Das, F. Rahaman, S. Ray. "Gravastars in $f(R,T)$ gravity," Phys. Rev. D95, 12, 124011 (2017). https://doi.org/10.1103/PhysRevD.95.124011
35. S. Pradhan, S. Mandal, P.K. Sahoo, Gravastar in the framework of symmetric teleparallel gravity. Chin. Phys. C **47**(5), 055103 (2023)
36. S. Pradhan, D. Mohanty, P.K. and Sahoo, Thin-shell gravastar model in $f(q,t)$ gravity. Chin. Phys. C **47**(9), 095104 (2023)
37. U. Debnath, Charge gravastars in $f(t)$ modified gravity. Eur. Phys. J. C **79**, 1–9 (2019)
38. M. Sinha, S. Surendra Singh, Gravastar model in the structure of $f(R,L_m,T)$ modified theory of gravity, Modern Physics Letters A 40, 05n06, 2450227, 0217–D7323 (2025). https://doi.org/10.1142/S0217732324502274
39. Z. Yousaf, Phys. Dark Univers. **28**, 100509 (2020)
40. M.Z. Bhatti, Mod. Phys. Lett. A **35**, 2050069 (2020)
41. C. Brandt, R. Chan, M. Silva, P. Rocha, J. Mod. Phys. **4**, 869–878 (2013)
42. S. Ghosh, F. Rahaman, B.K. Guha, S. Ray, Phys. Lett. B **767**, 380–385 (2017)
43. Z. Yousaf, K. Bamba, M.Z. Bhatti, U. Ghafoor, Charged gravastars in modified gravity. Phys. Rev. D **100**(2), 024062 (2019)
44. D. Bhattacharjee, P.K. Chattopadhyay, Stable charged gravastar model in cylindrically symmetric space-time. Phys. Scr. **98**(8), 085013 (2023)
45. A.A. Usmani, F. Rahaman, P.K.F. Kuhfittig, A. Rakib, Phys. Lett. B **701**, 388 (2011)
46. O. Sokoliuk, S. Pradhan, P.K. Sahoo, A. Baransky, Buchdahl quark stars within $f(q)$ theory. Eur. Phys. J. Plus **137**(9), 1–15 (2022)
47. A. Kumar Prasad, J. Kumar, Charged analogues of isotropic compact stars model with buchdahl metric in general relativity. Astrophys. Space Sci. **366**, 26 (2021). https://doi.org/10.1007/s10509-021-03931-9. arXiv:1910.10471 [physics.gen-ph]
48. R. Sharma, A. Ghosh, S. Bhattacharya, S. Das, Anisotropic generalization of buchdahl bound for specific stellar models. Eur. Phys. J. C **81**(6), 527 (2021)
49. S. Bhattacharya, R. Sharma, S.D. Maharaj, Electromagnetic extension of buchdahl bound in $f(r,t)$ gravity. Eur. Phys. J. C **84**, 64 (2024). https://doi.org/10.1140/epjc/s10052-024-12391-8
50. S. Ghosh, D. Shee, S. Ray, F. Rahaman, B.K. Guha, Gravastars with Kuchowicz metric potential, Results in Physics, Volume 14, 102473. ISSN 2211–3797 (2019). https://doi.org/10.1016/j.rinp.2019.102473
51. Y.B. Zel'dovich, Mon. Not. R. Astron. Soc. **160**, 1 (1972)
52. T.M. Braje, R.W. Romani, Astrophys. J. **580**, 1043 (2002)
53. L.P. Linares, M. Malheiro, S. Ray, Int. J. Mod. Phys. D **13**, 1355 (2004)
54. G. Darmois, Memorial des sciences mathématiques **25**, 58 (1927)
55. W. Israel, Nuo. Cim. **B44**, 1 (1966)
56. W. Israel, erratum-ibid, 48, 463 (1967)
57. H. Kim, B.H. Lee, W. Lee, Y.J. Lee, D.H. Yeom, Nucleation of vacuum bubbles in brans-dicke type theory. Phys. Rev. D **84**, 023519 (2011). https://doi.org/10.1103/PhysRevD.84.023519. arXiv: 1011.5981 [hep-th]
58. B.H. Lee, W. Lee, D.H. Yeom, Dynamics of false vacuum bubbles in brans-dicke theory. JCAP **01**, 005 (2011). https://doi.org/10.1088/1475-7516/2011/01/005. arXiv:1006.3127 [gr-qc]
59. K. Lanczos, Ann. Phys. (Berlin) **379**, 518 (1924)
60. N. Sen, Ann. Phys. (Leipzig) **378**, 365 (1924)
61. G.P. Perry, R.B. Mann, Gen. Relat. Gravit. **24**, 305 (1992)
62. P. Musgrave, K. Lake K., Class. Quant. Gravit. **13**, 1885 (1996)
63. A.T. Shafeek, M.A. Bakry, G.M. Moatimid, Gravastars in $f(r,\sigma,t)$ strong-gravity and antigravity theories. Pramana **97**(4), 189 (2023). https://doi.org/10.1007/s12043-023-02665-3
64. H.A. Buchdahl, General relativistic fluid spheres. Phys. Rev. **116**, 1027 (1959)
65. N. Straumann, *General Relativity and Relativistic Astrophysics* (Springer, Berlin, 1984)

66. C.G. Böhmer, T. Harko, Bounds on the basic physical parameters for anisotropic compact general relativistic objects. Class. Quant. Gravit. **23**, 6479 (2006). [arXiv:gr-qc/0609061]
67. B.V. Ivanov, Maximum bounds on the surface redshift of anisotropic stars. Phys. Rev. D **65**, 104011 (2002). [arXiv:gr-qc/0201090v2]
68. D.E. Barraco, V.H. Hamity, Maximum mass of a spherically symmetric isotropic star. Phys. Rev. D **65**, 124028 (2002)
69. M. Sharif, S. Naz, Eur. Phys. J. Plus **137**, 4 (2022)
70. H. Abreu et al., Class. Quant. Gravit. **24**, 4631 (2007)
71. U. Debnath, Charged gravastars in rastall-rainbow gravity. Eur. Phys. J. Plus **136**(4), 1–23 (2021)